Biomed Microdevices (2007) 9:719–727
DOI 10.1007/s10544-007-9081-3

Localization to atherosclerotic plaque and biodistribution of biochemically derivatized superparamagnetic iron oxide nanoparticles (SPIONs) contrast particles for magnetic resonance imaging (MRI)

Bryan R. Smith · Johannes Heverhagen · Michael Knopp · Petra Schmalbrock · John Shapiro · Masashi Shiomi · Nicanor I. Moldovan · Mauro Ferrari · Stephen C. Lee

Published online: 12 June 2007

Abstract Annexin V recognizes apoptotic cells by specific molecular interaction with phosphatidyl serine, a lipid that is normally sequestered in the inner leaflet of the cell membrane, but is translocated to the outer leaflet in apoptotic cells, such as foam cells of atherosclerotic plaque. Annexin V could potentially deliver carried materials (such as superparamagnetic contrast agents for magnetic resonance imaging) to sites containing apoptotic cells, such as high grade atherosclerotic lesions, so we administered biochemically-derivatized (annexin V) superparmagnetic iron oxide particles (SPIONs) parenterally to two related rabbit models of human atherosclerosis. We observe development of negative magnetic resonance imaging (MRI) contrast in atheromatous lesions and but not in healthy artery. Vascular targeting by annexin V SPIONs is atheroma-specific (i.e., does not occur in healthy control rabbits) and requires active annexin V decorating the SPION surface. Targeted SPIONs produce negative contrast at doses that are 2,000-fold lower than reported for non-specific atheroma uptake of untargeted superparamagnetic nanoparticles in plaque in the same animal model. Occlusive and mural plaques are differentiable. While most of the dose accumulates in liver, spleen, kidneys and bladder, annexin V SPIONs also partition rapidly and deeply into early apoptotic foamy macrophages in plaque. Contrast in plaque decays within 2 months, allowing MRI images to be replicated with a subsequent, identical dose of annexin V SPIONs. Thus, biologically targeted superparamagnetic contrast agents can contribute to non-invasive evaluation of cardiovascular lesions by simultaneously extracting morphological and biochemical data from them.

Keywords Vascular imaging · Molecular imaging · Targeted contrast · Apoptosis · Annexin V · Superparamagnetic

B. R. Smith · J. Shapiro · N. I. Moldovan
Department of Biomedical Engineering, Ohio State University, 1080 Carmack Road, Columbus, OH 43210, USA

J. Heverhagen · M. Knopp · P. Schmalbrock
Department of Radiology, Ohio State University, 630 Means Hall, 1654 Upham Drive, Columbus, OH 43210, USA

M. Shiomi
Institute for Experimental Animals, Kobe University Graduate School of Medicine, Kobe, Japan

M. Ferrari
Brown Institute of Molecular Medicine, Department of Biomedical Engineering, The University of Texas Health Science Center, 1825 Pressler, Suite 537D, Houston, TX 77031, USA

S. C. Lee (✉)
Departments of Biomedical Engineering, Chemical and Biomolecular Engineering, Cellular and Molecular Biochemistry, Davis Heart and Lung Research Institute, Ohio State University, 473 W. 12th Ave., Columbus, OH 43210, USA
e-mail: lee.1996@osu.edu

1 Introduction

Atherosclerosis affects much of the Western population (Kolodgie et al. 2004; Naghavi et al. 2003; Meuwissen et al. 2003; Cui et al. 2005) and disease is often

symptomatically silent until a catastrophic vascular event (myocardial infarction, stroke, arterial dissection, etc.). Coupled with the insidious nature of developing atherosclerosis, the excellent outcomes of pre-event therapy (Kolodgie et al. 2003a,b; Bhatia et al. 2003; Strauss et al. 2004) suggest that non-invasive detection of patients at high risk for imminent cardiovascular events would be beneficial. Identification of patients at risk for imminent vascular events requires screening of largely disease-free or asymptomatic populations, so low morbidity imaging methods, like CT (computerized tomography) or MRI (magnetic resonance imaging), would seem ideal (Kolodgie et al. 2003b). The possibility that MRI might utilize contrast agents that are targeted by biochemical affinity to particular lesional macromolecules offers the potential to extract very specific information about chemical content of plaque and, as we show here, information regarding the physiological state of cellular constituents of plaque (i.e., apoptotic cells). The opportunity to extract biochemical and pathophysiological information of similar quality and specificity is largely absent from other (cheaper) high resolution imaging modalities, such as CT.

MRI-based evaluation of the risk posed by individual lesions will require determination/consideration of multiple parameters. Parameters will include location of atherosclerotic lesions in the vascular tree, reading on the likely consequences of thrombotic occlusion at those sites. Furthermore, atherosclerotic lesions are differentiated by the stage of disease they represent (Kolodgie et al. 2003b; Bhatia et al. 2003; Strauss et al. 2004), with so-called vulnerable plaque presenting the highest risk for catastrophic thrombosis. Differentiating features of vulnerable plaque include plaque morphology and structure (thin fibrous caps over large lipid-containing cores, sometimes plaques with non-occlusive morphology), as well as cellular and biochemical composition (heavy infiltration of macrophages that are often apoptotic, high concentrations of molecules associated tissue remodeling and inflammation, plaques with large necrotic cores etc. (Cui et al. 2005; Bhatia et al. 2003; Hegyi et al. 2001; Libby et al. 1995)). In principal, location of plaque in vasculature, the gross morphology of plaque and the chemical composition of plaque might be addressed minimally invasively by MR imaging, providing there are available contrast agents that can access and specifically direct contrast to plaque biochemical constituents indicative of vulnerability.

Here we target superparamagnetic iron oxide nanoparticles (SPIONs, providing negative contrast) to arterial lesions using annexin V. Annexin V recognizes cells by binding phosphatidyl serine (PS) in outer leaflets of cell membranes and binds plaque in hyperlipidemic rabbits (Kolodgie et al. 2003a; Li et al. 2004; Shiomi et al. 2003). Cell types that bind annexin V include apoptotic cells, activated platelets and nonapoptotic, lipid-loaded cells, all of which are found in plaque (Lupu et al. 1993; Moldovan et al. 1994). Furthermore, high burdens of cells presenting PS in their membrane outer leaflets have been positively correlated with high grade, vulnerable plaque (Kolodgie et al. 2003a; Li et al. 2004; Shiomi et al. 2003).

2 Materials and methods

2.1 Animals

We used models genetically predisposed to atherosclerosis and based on the Watanabe heritable hyperlipidemic (WHHL) rabbit strain. WHHL rabbits were from Covance (Princeton, NJ) and Watanabe Heritable Hyperlipidemic Myocardial Infarction (WHHLMI), rabbits were provided by collaborator M. Shiomi (Kobe University). WHHLMIs have all the features of WHHLs, but also spontaneously suffer myocardial infarction (Li et al. 2004; Ito et al. 2004). New Zealand White rabbits were used as disease-free controls (Covance).

2.2 Superparamagnetic nanoparticles

SPIONs consisting of an iron oxide core coated with dextran and conjugated to a protein (annexin V or protein G) were obtained from Miltenyi Biotec (Gladbach, Germany). SPIONs were purified and concentrated using a high-gradient magnetic separation apparatus (Miltenyi Biotec). One half to 2 ml of annexin V or Protein G SPION stock suspensions were placed in a high gradient magnetic field overnight. After decanting supernatants, SPIONs were washed twice with PBS (Invitrogen, Carlsbad, CA) and magnetically separated again.

2.3 SPION characterization

SPIONs were characterized for protein and iron concentration as well as annexin V bioactivity. Protein content was determined by bicinchoninic acid (BCA) assay (Smith et al. 1985) from Pierce Chemical Company (Rockford, IL).

Mass of iron in samples was quantified spectrophotometrically (Riemer et al. 2004). SPION size was determined in PBS following sonication to eliminate aggregates. Particles were sized by hydrodynamic diameter via Dynamic Light Scattering (DLS) with a Zetasizer Nano S Series instrument from Malvern Instruments (Southborough, MA).

Bioactivity of annexin V SPIONs was determined by comparing the binding of particles to apoptotic Jurkat cells versus normal Jurkat cells. Apoptosis was induced in Jurkat cells by camptothecin (20 μg/ml, (Schellenberger et al. 2002), and verified in camptothecin-treated cells by

TUNEL assay. Cells received 20 μl annexin V conjugated SPIONs and $CaCl_2$ to 20 mM. Control lots of cells also received EDTA (100 mM) to chelate Ca^{+2} (Ca^{+2} is necessary for annexin V binding). Other control lots of cells received exogenous PS (C-8, 5 μg/ml Avanti Polar Lipids, Alabaster, AL) to competitively inhibit annexin V binding of apoptotic cells. Annexin V SPION-bound cells were isolated magnetically and quantified by Coulter Counter.

2.4 Magnetic resonance imaging

MRI was performed with a 4.7 T small animal MRI system (Biospin, Bruker, Etlingen, Germany). Anesthesia was induced by intramuscular injection of a combination of 20 mg/kg ketamine and 1 mg/kg diazepam and maintained inhalation of 2% isofluorane. Rabbits were placed supine in the scanner to minimize breathing artifacts.

The imaging protocol used a three plane localizer, time of flight angiography of the abdominal aorta, and an axial, fat-saturated, gradient echo sequence (repetition time: 1,230 ms; echo time: 11.1 ms; flip angle: 30°; Slice thickness: 3 mm; field of view: 90×90 mm; Matrix 256×256; number of excitations: 1; acquisition time: 5 min and 16 s). Aliquots of SPIONs containing 0.05 mg of iron were injected into an ear vein, followed immediately by a 1 ml bolus of sterile saline. The gradient echo sequence was carried out before injection and repeated at 5, 10, 15, 20 and 60 min after injection of SPIONs.

2.5 Histology and electron microscopy

To confirm the presence of SPIONs in aortic segments, WHHL and WHHLMI rabbits whose MRI images are shown were sacrificed 1 h after administration of SPIONs in their final imaging sessions. We also sacrificed control WHHLMI and WHHL animals who had never received SPIONs for comparative histological analysis. Whole aortas were resected, fixed in 10% formalin solution, and examined by pathologists on both gross and microscopic levels. Also, small slices of aorta from the imaged region of WHHLMI aorta were fixed in 3% glutaraldehyde for transmission electron microscopy (TEM). Segments of excised aorta where MRI signal cancellation was observed were embedded in paraffin and 4 μm sections were cut and stained. Segments of aorta that did not exhibit contrast in MRI were also mounted in paraffin and sectioned. In both sets of histology sections, Prussian blue with eosin counterstained was used to detect iron. A TUNEL apoptosis detection kit (Calbiochem, San Diego, CA, (Gavrieli et al. 1992) and Hoechst stain (Hoechst 33342, Sigma, St. Louis) were to used to detect apoptosis. TUNEL stains were counterstained with methyl green (to differentiate non-apoptotic nuclei from apoptotic nuclei).

2.6 Magnetoradioisotopic annexin V SPIONs

We used annexin V SPIONs labeled with Technetium-99 m (^{99}Tc) to follow biodistribution. Two ml (0.054 mg/ml iron, approx. 30 μg/ml annexin V) of magnetically concentrated annexin V SPIONs were labeled as described using ethylenedicysteine (ABX chemicals, Germany) N-Hydroxysulfosuccinimide (Pierce, Rockford, IL) and Ethyl-3-(3-dimethylaminopropyl)-carbodiimide (EDC, Sigma, St. Louis). After 24 hours, the EC- annexin V SPIONs were magnetically separated, resuspended in PBS, quantified for iron content (as described) and stored at 4°C. One to 2 h prior administration of labeled annexin V SPIONs in vivo, 15 mCi of ^{99}Tc-pertechnetate and 60 μg $SnCl_2$ were added to an aliquot of EC-annexin V SPIONs containing 0.05 mg iron. ^{99}Tc-labelled annexin V SPIONs were separated from unincorporated label by size exclusion chromatography. Specific activity was determined by gamma counter.

2.7 SPECT/CT imaging

We followed biodistribution of radiolabeled annexin V SPIONs by SPECT/CT (single positron emission computerized tomography/computerized tomography). SPECT imaging was performed by Forte gamma camera (Phillips Medical Systems, Milpitas, CA) with a 64×64×16 matrix. 128 frames were obtained over a 360° orbit at 35 s/frame and a 1.46 zoom. An order 6, 0.43 cut-off Butterworth filter was used for image processing. Anesthesia was as for MRI and the urethra was catheterized. Magnetoradioisotopic ^{99}Tc-Annexin V SPIONs (labeled as described above) were injected intravenously as for MR imaging, and two consecutive 30 min scans were performed.

A 16 slice Siemens computed tomography (CT) scanner (Siemens AG, Forchheim, Germany) with 200 mAs and 120 kVp, using 3 mm×3 mm reconstructions was employed for anatomical co-registration of the rabbit with SPECT. A Kernel B31f was applied for medium smoothing. SPECT and CT images were fused and evaluated by OSU radiologists and technicians.

2.8 Data analysis and interpretation

MRI images were analyzed using Medical Image Processing, Analysis and Visualization (MIPAV) (McAuliffe et al. 2001). Visual analysis of MRI images was performed by two physicians with MRI experience and by a veterinarian specializing in radiology, in consensus. Regions of interest

(ROI) were placed in the aorta, liver, kidney, and paraspinal muscle. Average signal intensities in these ROIs and its percent change over time were calculated.

3 Results

3.1 Particle characterization

Miltenyi SPIONs are reported to contain single 10–12 nm iron oxide grains (Ahrens et al. 2003), and based on mean diameters of iron grains and average of densities of Fe_3O_4 and Fe_2O_3, and our iron assay, we estimated the numbers of particles/ml in stocks. Iron content was 0.05 mg/ml for annexin V SPIONs and 0.5 mg/ml for protein G SPIONs (Table 1). Dynamic light scatter indicated diameters of 90 and 100 nm, respectively, for protein G and annexin V SPIONs in PBS. Protein content of both types of nanoparticles were similar (about 30 μg/ml, Table 1). Given the similar sizes of protein G and annexin V and our estimated SPION concentrations, the mean number of proteins/particle was 10-fold higher for annexin V SPIONs. To bring all of the SPIONs used to comparable concentrations, particles were purified by magnetic separation (as per the manufacturer) and resuspended in PBS to a final iron concentration of about 0.05 mg/ml.

Bioactivity of annexin V was confirmed by the ability of nanoparticles to drive magnetic separation of cells that had been made apoptotic with camptothecin (and therefore had annexin V's ligand (PS), in the outer leaflet of their cell membranes, see Table 2). Non-apoptotic cells were not magnetically separable with annexin V SPIONs. Separation of apoptotic cells did not occur if Ca^{+2} (required for annexin V-PS binding) is chelated, nor did separation occur in the presence of free, exogenous PS. We conclude that binding to apoptotic cells depended on bioactive annexin V on the USPIOs.

3.2 WHHL rabbit MRI

Atherosclerotic lesions can contain multiple cell types (Cui et al. 2005; Bhatia et al. 2003; Hegyi et al. 2001; Libby et al. 1995; Lupu et al. 1993; Moldovan et al. 1994), which might bind annexin V-conjugated SPIONs. Annexin V nanoparticles were injected into the Watanabe heritably hyperlipidemic rabbit (WHHL, Ruehm et al. 2001). Animals used were retired breeders (1–2 years old) with advanced atherosclerosis (see below). New Zealand white rabbits of comparable age were imaged identically as atherosclerosis-free negative controls. We chose an anatomical region which was convenient for repeated MR imaging (abdominal aorta, distal to renal arteries). The region is easy to find, is not subject to motion artifacts, and consistently develops atherosclerotic lesions in WHHLs. Resolution achieved for rabbits shown in Fig. 1 was typical of the MRI images shown in this paper. Specifically, in-plane resolution is approximately 90/256 (0.35 mm/pixel) in the images shown with a slice thickness/gap of about 3/2 mm.

Annexin V SPIONs, but not protein G SPIONs, mediated rapid contrast development in WHHL rabbits (Fig. 1, Table 3). The aortic region of interest of both WHHL animals was highly occluded compared to the same region of New Zealand white aorta (Fig. 1). Due to limited MRI resolution and high level of constriction of the infrarenal aorta in WHHLs, annexin V SPION-mediated signal cancellation apparently filled the lumenal volume. Contrast in both WHHLs was quantitatively similar (Table 3). Signal cancellation was apparent 5 min post-injection reaching a plateau at 15 min that was sustained for the remainder of the 1 h imaging experiment (Fig. 1, Table 3). These comparisons are valid as within an imaging experiment, background remained constant as animals were not removed from the scanner until the experiment was completed.

No signal cancellation was observed in the New Zealand white animals after administration of annexin V SPIONs or protein G SPIONs (Fig. 1, Table 3) over the 60 min duration of the experiment.

We tested whether annexin V SPIONs could be used for repeated imaging of a single animal. The WHHL rabbit shown in Fig. 1 was administered a second identical dose of annexin V SPIONs and re-imaged 70 days after the initial

Table 1 Iron and protein content and particle diameter of annexin V and protein G SPIONs

Nanoparticles	Iron (mg/ml)	Protein (μg/ml)	Particle size (nm)	Particles/ml
Annexin V SPIONs	0.054	29.2	98	4×10^{13}
Protein G SPIONs	0.478	27.5	90	4×10^{14}

Table 2 Annexin V on SPIONs is bioactive

Treatment conditions Campothecin	PS	EDTA	Annexin V SPIONs	Cells isolated magnetically ($\times10^3$)
+	−	−	+	67
−	−	−	+	4
+	−	+	+	1
+	+	−	+	6

PS Phosphotidylserine, *EDTA* Disodium EDTA.

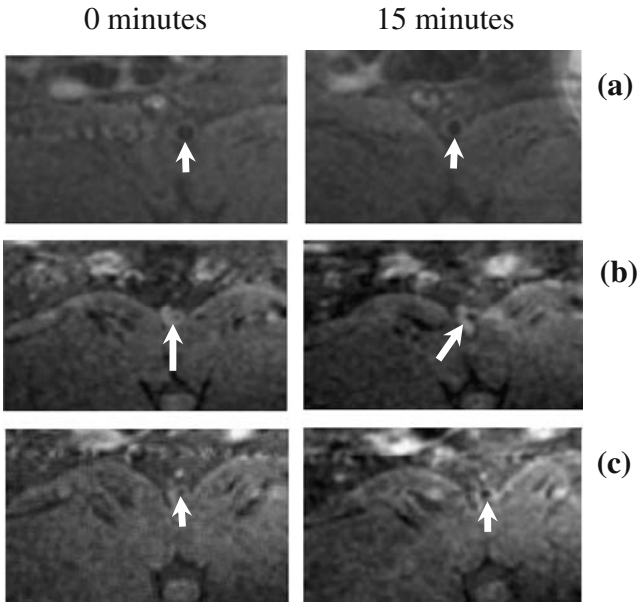

Fig. 1 Annexin V SPIONs deliver negative contrast to the abdominal aorta of WHHL rabbits, but not to the abdominal aorta of New Zealand White rabbits. Transverse images of abdominal aorta between the renal and femoral arteries taken at 0 min (before administration of annexin V SPIONs), and 15 min after are shown. Row (**a**) images are derived from a New Zealand White rabbit (negative control animal, imaging day 0), images labeled (**b**) are derived from a WHHL rabbit (WHHL 1, imaging day 0) and images labeled (**c**) are derived from the same WHHL rabbit as seen in (**b**), but at a subsequent date (WHHL 1, Table 3, imaging day 70). A dose of annexin V SPIONs identical to that used on day 0 were re-administered to WHHL 1 70 days after first administration, and WHHL 1 was re-imaged using the protocol used on day 0. *Arrows* indicate abdominal aorta and sites of signal cancellation. The WHHL rabbit exhibited obvious concentric narrowing of the aorta: the luminal area of the New Zealand White rabbit is much larger than that of the WHHL rabbit

experiment. Prior to re-administration of annexin V SPIONs, contrast from the previous experiment was no longer evident (Data not shown).

Annexin V SPION-mediated contrast development was quantitatively and kinetically similar to that observed 70 days earlier in the first administration of annexin V SPIONs to that animal (Fig. 1, Table 3).

3.3 WHHLMI rabbit MRI

Recently, Shiomi et al. 2003 described a variant of the WHHL, the Watanabe heritable hyperlipidemic myocardial infarction (WHHLMI) rabbit. The WHHLMI features a higher plaque burden in *coronary* arteries than WHHLs (Ruehm et al. 2001), plaques with morphologies that resemble those of human vulnerable plaques, and spontaneous myocardial infarctions. Twelve to 16 month old WHHLMIs were imaged using the annexin V SPIONs and imaging protocols used for the WHHLs and New Zealand white rabbits.

In WHHLMI rabbits, Annexin V-targeted SPIONs directed contrast at the abdominal aorta, as in WHHLs (Fig. 2, Table 3). Contrast delivery in the abdominal aorta of two distinct WHHLMI rabbits were similar to each other (Fig. 2, Table 3), but distinct from WHHLs (Fig. 1, Table 3). The abdominal aortic lumens of WHHLMIs were less occluded than WHHLs (Fig. 2). Signal cancellation occurred in WHHLMI in a periannular distribution around the aortic lumen. Figure 2 demonstrates concurrent extraction of biochemical (the presence of accessible PS in plaque) and morphological information (the mural morphology of the plaque). Mural plaque morphology presents a detection challenge for purely lumenographic methods, and flat morphology can be an important feature in evaluation of the vulnerability of plaque (Kolodgie et al. 2003b; Bhatia et al. 2003; Strauss et al. 2004). Image resolution in Fig. 2 was similar to that observed for rabbits of Fig. 1.

3.4 Histology: SPION localization to imaged plaques

Presence of atheroma in imaged regions of WHHL and WHHLMI aorta (Figs. 1, 2, Table 3) was confirmed histologically. New Zealand white aortic segments were histologically normal, but atheroma was readily apparent in WHHL and WHHLMIs aortas distal to the renal arteries. Two independent pathologists examined resected hyperlidemic rabbit aortas and concurred lesions in the

Table 3 Change in MRI signal in the abdominal aorta of rabbits receiving targeted SPIONs

Animal/SPION type	Signal change after injection of SPIONs (%)		
	Imaging day	5 min	15 min
WHHL 1/annexin V	0	−9	−11
WHHL 1/annexin V	70	−7	−11
WHHL 1/protein G	0	+4	+1
WHHL 2/annexin V	0	−18	−16
WHHLM 1/annexin V	0	−24	−23
WHHLM 2/annexin V	0	−21	−24
WHHLM 1/protein G	0	−3	+1
New Zealand White/annexin V	0	−1	+2

WHHL Watanabe heritably hyperlipidermic rabbit, *WHHLMI* Watanabe heritably hyperlipidermic spontaneous myocardial infarction rabbit.

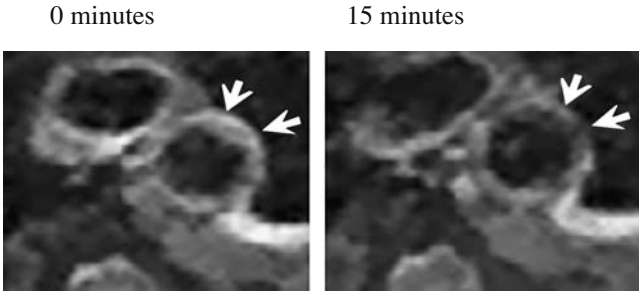

Fig. 2 Annexin V SPIONs deliver negative contrast to the abdominal aorta of WHHLMI hyperlipidemic rabbits. Transverse images of abdominal aorta between the renal and femoral arteries taken at 0 min (before administration of annexin V SPIONs) and 15 min after are shown. WHHLMI 1 is shown (Table 3). *Arrows* indicate abdominal aortic plaque and sites of signal cancellation

MRI-imaged region had subintimal expansion of uniform thickness, containing numerous acicular (cholesterol) clefts in both WHHL and WHHLMI animals. Foamy macrophages, abnormal smooth muscle cells and distributed mineral deposits were noted, again in both WHHLs and WHHLMIs. Lesions were classified type III because they lacked necrotic cores and fibrous caps, though they had some type IV characteristics (apoptotic macrophages and mineral deposits, Ruehm et al. 2001), the presence of which were most pronounced in WHHLMI rabbit lesions.

Histologic analysis of a section of abdominal aorta from WHHLMI Rabbit 1 (taken from region exhibiting contrast in Fig. 2) is shown in Fig. 3. Prior to sacrifice, aortic resection and histology, the animal received annexin V SPIONs at doses used in MRI.

Iron was detected in sections by Prussian blue staining, and the strongest staining occurred in pockets of foamy cells deep in the plaque (Fig. 3). TUNEL (Gavrieli et al. 1992) showed some of the Prussian blue staining foamy macrophages were in early apoptosis (Fig. 3(c), brown nuclei) while others were not (Fig. 3(c) green nuclei). Nuclear fragmentation/compaction was observed infrequently, though an example of such from the macrophage pocket is shown in the Hoecst assay of Fig. 3(d). In addition to macrophages, Hoecst and TUNEL assay revealed apoptotic smooth muscle cells distributed throughout the pathological intima, though these cells did not stain heavily with Prussian blue (Data not shown).

The presence of SPIONs deep in plaque was corroborated by Transmission Electron Microscopy (TEM). TEM revealed electron-dense particles the size of annexin V SPIONs deep in the same atherosclerotic plaque imaged by light microscopy above (Fig. 4). As expected, SPIONs are commonly seen in association with cell membranes (arrows in Fig. 4(b)). Electron dense structures too large to be single annexin V nanoparticles occur in several locations in the lower magnification plaque image (Fig. 4(a)), and may be aggregates of SPIONs (as seen in inset of Fig. 4(b)). Voids in the TEM image often occurred near sites where SPIONs were detected and may be due to extracellular cholesterol crystals that were dissolved away during processing for TEM.

3.5 Whole body distribution of annexin V SPIONs

A key utility for targeted contrast agents is non-invasive atherosclerotic disease staging in vivo, so understanding biodistribution of annexin V targeted SPIONs is essential. To follow biodistribution of the targeted particles, annexin V SPIONs were radiolabeled with ^{99}Tc (Riemer et al. 2004) and a quantity of radiolabeled particles containing 0.05 mg of iron was injected into the imaged WHHLMI Rabbit 2 (Table 3). Administered ^{99}Tc-labeled annexin V SPIONs (4.8 mCi/4×10^{13} particles) contained no more than 5–10% free ^{99}Tc, determined by size exclusion chromatography. A SPECT/CT fused image of the WHHLMI collected 30 min after receiving labeled compound is shown in Fig. 5.

Radiolabel was present in kidneys, bladder, liver and spleen, with abdominal aorta poorly (if at all) detectable in this experiment. Thus, most of the annexin V SPIONs went to spleen and liver, as previously reported (Weissleder et al. 1990a,b). Free ^{99}Tc is eliminated via the urinary tract, so accumulation of radioactivity there (kidney, bladder) is not

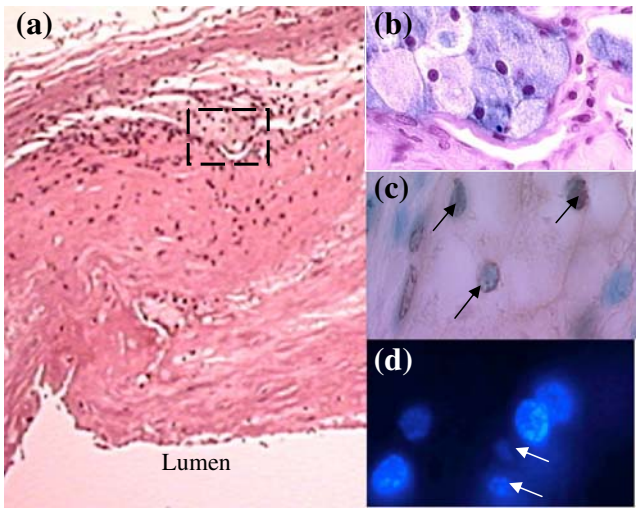

Fig. 3 Annexin V SPIONs are present in the plaque from the imaged regions of abdominal aorta. Histologic section abdominal aorta of the WHHLMI rabbit 1 (see Fig. 2) following imaging is shown. Image is a hematoxylin–eosin stain of a representative section of the region of contrast delivery (40× magnification). An adjacent section was stained for iron (*Prussian blue*, image (**b**), 400× magnification). The cells staining with *Prussian blue* have morphologies characteristic of foamy macrophages. Image (**c**) shows TUNEL assay of cells from the same pocket of macrophages (apoptotic nuclei staining *brown*, indicated with *black arrows*, non apoptotic nuclei staining with *methyl green*). Image (**d**) shows Hoechst stain of the *Prussian-blue* staining macrophages with possible fragmented nuclei noted (*white arrows*)

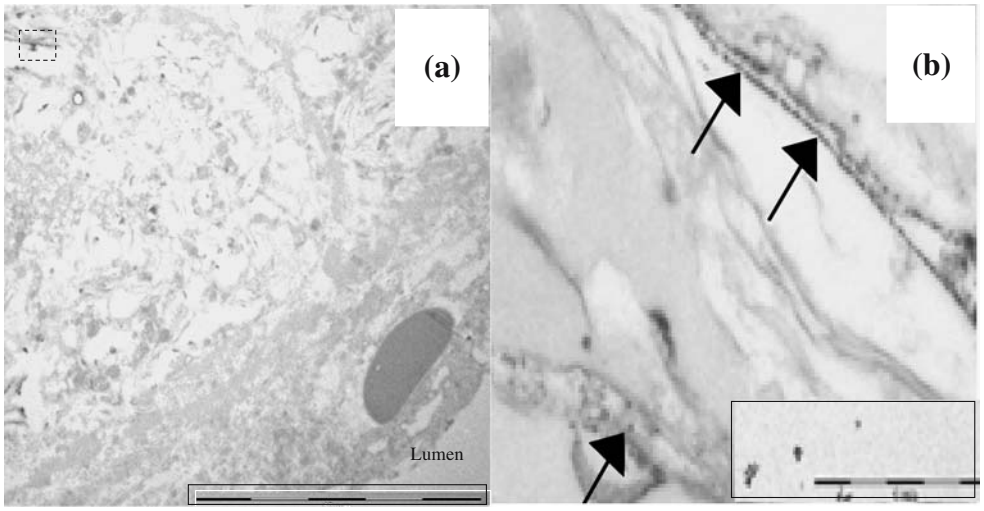

Fig. 4 Transmission electron microscopy shows SPIONs in WHHLMI plaque. Image (**a**) shows a segment of WHHLMI rabbit 1 abdominal aorta near the histological section shown in Fig. 3 magnified 1,000× (10 μm size *bar* inset). The *dashed box* of image (**a**) was further enlarged to 20,000× final magnification in image (**b**) (1 μm size *bar* in inset). The inset image shows a 20,000× magnification of annexin V SPIONs spread on a TEM stage for size comparison. Particles the size of annexin V SPIONs seen in the inset that are associated with cells of WHHLMI plaque and are indicated by *arrows* in image (**b**)

surprising in light of low amounts of free ^{99}Tc in the radiolabelled annexin V superparamagnetic nanoparticles.

3.6 Tolerability of annexin V SPIONs

Annexin V SPIONs are apparently well-tolerated by rabbits at the doses used. None of the animals receiving nanoparticles exhibited detectable symptoms of systemic toxicity attributable to SPIONs (malaise, fever, etc., data not shown). Since SPECT/CT showed that annexin V SPIONs concentrated primarily in the RES, RES organs (spleens, livers) of rabbits receiving and not receiving annexin V SPIONs were resected, sectioned for histology and stained with eosin and Prussian blue. Pathologists noted no recipients of SPIONs exhibited no pathological changes in their RES organs relative to the RES organs of animals that did not receive SPIONs (Data not shown).

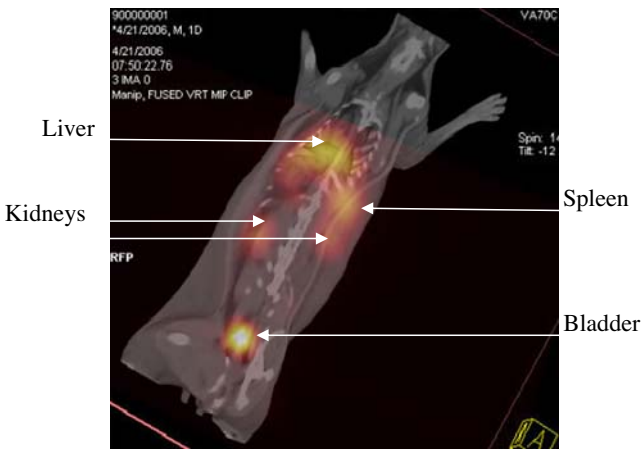

Fig. 5 Most annexin V SPIONs distribute to locations other than the abdominal aorta. Annexin V on SPIONs was labeled with ^{99}Tc and injected into a WHHL rabbit. Organs accumulating radiolabel are indicated

4 Discussion

Cheap, reliable screening for vulnerable plaque could significantly improve the well-being of the Western population, if implemented widely, and our goal is development of a non-invasive method to detect vulnerable plaque prior to rupture in humans, in vivo. Ideally, the screening system would determine location, morphology and critical molecular content of plaque to identify dangerous lesions in time for interventions that preclude debilitating consequences of rupture. Untargeted superparamagnetic nanoparticles can deliver negative contrast to atherosclerotic lesions, documenting plaque location and to some extent, morphology (Ruehm et al. 2001). Incorporation of a biochemical affinity (targeting) reagent in the contrast agent can potentially add an additional dimension to assessment of plaque vulnerability, that being plaque biochemical composition. In this context, we evaluated annexin V SPIONs in two related rabbit models of atherosclerosis.

The SPIONs partitioned into arterial lesions: targeting of annexin V SPIONs were congruent with the known binding properties annexin V and biology of atheroma (Kolodgie et al. 2003a; Li et al. 2004; Shiomi et al. 2003). Signal

cancellation occurred in neither the aortas of New Zealand white (i.e., disease-free) rabbits receiving annexin V SPIONs nor in hyperlipidemic rabbits receiving protein G (untargeted) SPIONs. Observed signal cancellation was correlated to presence of SPIONs in plaque. At arterial lesions exhibiting signal cancellation, iron of SPIONs was detected by Prussian blue staining and the nanoparticles themselves were directly detectable by electron microscopy. Targeting was due to PS interaction with annexin V decorating the SPIONs: nanoparticle-associated annexin V was biologically active before administration in vivo, and annexin V SPIONs were associated with lipid-engorged macrophages. Foamy macrophages have the annexin V ligand PS in the outer leaflets of their membranes (Lupu et al. 1993; Moldovan et al. 1994). Furthermore, some macrophages taking up annexin V SPIONs also gave TUNEL and Hoecst assay results consistent with early apoptosis.

Several of the properties of the annexin V SPIONs in vivo bear discussion. First, targeting allowed detection using small amounts of contrast agent. Annexin V SPIONs detected plaque in rabbits at doses almost 2,000-fold lower than reported for untargeted superparamagnetic particles on a mg iron/kg body weight basis (Ruehm et al. 2001). While the untargeted particles and our nanoparticles have different sizes and surface chemistries (Ruehm et al. 2001), the reduction in required dosing observed is large. Furthermore, at the dosing level used, the animals did not exhibit any systemic toxicity correlated to SPION administration, nor did resected RES organs of SPION recipients exhibit any pathology relative to untreated animals.

Reduction in dosing *in vivo* required to achieve a specific therapeutic effect can occur with targeted delivery of therapeutics (Goldin et al. 2001; Lee et al. 2004a,b; Duncan 1997a,b; Duncan et al. 2001; Jain 1998; Maeda et al. 2001) and is mediated by numerous factors including altered biodistribution, degradation and clearance properties associated with specific targeting. Whatever accounts for the imaging efficacy of low doses of annexin V SPIONs, the bolus of iron administered is 20-fold less than the maximum tolerated dose is in humans, suggesting significant dose acceleration may be feasible.

The foregoing is fortunate, as the dose of annexin V SPIONs apparently did not bind all PS in the rabbit vasculature. For instance, apoptotic smooth muscle cells were detectable in plaque by TUNEL assay (Data not shown), but they did not stain detectably with Prussian blue, indicating that they had not taken up annexin V SPIONs as well as did macrophages. Given that macrophages are professional phagocytes, and smooth muscle cells are not, this may be only as expected, and the inability to detect iron in apoptotic smooth muscle cells by Prussian blue may reflect differences in sensitivity in apoptosis detection by TUNEL and iron detection by Prussian blue.

Secondly, negative MRI contrast developed very rapidly (within 5 minutes of administration of annexin V SPIONs). The speed of contrast onset suggests that cells taking up particles were in the plaque at the start of the experiment. If annexin V SPIONs access apoptotic macrophages in plaque by passive diffusion from the arterial lumen, the rapidity of contrast development makes the observed deep plaque penetration by annexin V SPIONs remarkable. Alternatively, delivery of the particulate contrast agent may occur via the *vasa vasorum*, perhaps accounting for rapid penetration deep into plaque. Recently, cell trafficking into plaque has been reported to occur via *vasa vasorum* (Moreno et al. 2006), so perhaps it is not surprising should particulates such as annexin V SPIONs prove to enter by a similar route. We are currently investigating the mode of delivery of annexin V SPIONs.

Thirdly, contrast delivery can be replicated with repeat administration of annexin V SPIONs, which bodes well for repeat use of targeted superparamagnetic nanoparticles in screening. Decay of MRI contrast from previous imaging sessions is necessary if targeted nanoparticles are to be used repeatedly to follow progression of plaque over time. We have not fully defined the kinetics of loss of negative contrast from plaque, though we know it is gone within 70 days. Reliable detection of imminently vulnerable plaque may require monitoring multiple plaque parameters, including coincidence of multiple biochemical markers in single plaques (Bhatia et al. 2003; Nighoghossian et al. 2005; Stoneman and Bennett 2004), which might be accomplished by serial imaging with individually targeted contrast agents. If so, kinetics of decay of contrast from earlier rounds of imaging will determine time intervals between imaging sessions. We are working to define kinetics and mechanism of decay of annexin V superparamagnetic nanoparticles contrast from plaque.

Finally, radiolabeled annexin V SPIONs did not make the abdominal aorta clearly visible in SPECT/CT fused images, though it *is* clearly visible in MRI images. Most of the bolus of annexin V SPIONs distribute to the organs of the RES and the kidneys and bladder, congruent with biodistribution behavior of both annexin V (Kolodgie et al. 2003a; Li et al. 2004; Shiomi et al. 2003) and other dextran-coated superparamagnetic iron particles (Weissleder et al. 1990a,b). That the bolus goes primarily into RES and excretory organs may be a problem if annexin V SPIONs are used as a platform for simultaneous imaging and therapeutic administration to plaque (Goldin et al. 2001; Lee et al. 2004a,b). Toxicities to the RES organs could be a concern, though none were detected with the SPIONs at the dosing used here.

Plaques detected here by MRI meet broad definitions of vulnerable lesions (containing high contents of lipid and

apoptotic macrophages, mineral deposits, Naghavi et al. 2003; Kolodgie et al. 2003a; Strauss et al. 2004; Nighoghossian et al. 2005; Meuwissen et al. 2003; Hartung et al. 2005) and so our findings suggest that cardiovascular MRI using targeted SPIONs might be used to help identify dangerous lesions prior to thrombotic events. However, annexin V SPIONs are not likely alone be sufficient to the diagnostic task and the need for multi-parameter analysis for accurate evaluation of risk of acute vascular events and following disease progression is widely accepted. We have identified several other affinity regents which target SPIONs to the same region of aorta in hyperlipidemic rabbits, (Lee et al. in preparation, also Davies et al. 2005; Belizaire et al. 2003; Liu et al. 2003) so that a non-invasive system for cardiovascular disease staging based on targeted MRI contrast may be possible. While the challenges are significant, we are optimistic for the potential contribution of targeted superparamagnetic nanoparticles in non-invasive evaluation of vascular disease.

Acknowledgments The authors acknowledge George Hinkle, Charles Hitchcock, Nathan Hall, Noe Tirado-Muniz, Krista LaPerle and Donna Kusewitt for their technical support and advice. This work supported was by BRTT02-0001, a grant from the Biomedical Research and Technology Transfer Commission of Ohio and National Science Foundation Grant No. 0221678.

References

E.T. Ahrens, M. Feili-Hariri, H. Xu, G. Genove, P.A. Morel, Magn. Reson. Med. **49**, 1006–1013 (2003)

A.K. Belizaire, L. Tchistiakova, Y. St-Pierre, V. Alakhov, Biochem. Biophys. Res. Commun. **309**, 625–630 (2003)

V. Bhatia, R. Bhatia, S. Dhindsa, A. Virk, J. Postgrad. Med. **49**, 361–368 (2003)

Y. Cui, D. Zhao, H. Liu, Z. Ning, J. Yang, X. Qing, S. Yu, C. Wu, Maturitas **50**, 337–343 (2005)

J.R. Davies, J.F. Rudd, T.D. Fryer, P.L. Weissberg, J. Nucl. Cardiol. **12**, 234–246 (2005)

R. Duncan, Chem. Ind. **7**, 262–264 (1997a)

R. Duncan, J. Drug Target. **5**, 1–4 (1997b)

R. Duncan, S. Gac-Breton, R. Keane, R. Musila, Y.N. Sat, R. Satchi, F. Searle, J. Control. Release **74**, 135–146 (2001)

Y. Gavrieli, Y. Sherman, S.A. Ben-Sasson, J. Cell Biol. **119**, 493–501 (1992)

D.S. Goldin, C.A. Dahl, K.L. Olsen, L.H. Ostrach, R.D. Klausner, Science **292**, 443–445 (2001)

D. Hartung, M. Sarai, A. Petrov, F. Kolodgie, N. Narula, J. Verjans, R. Virmani, C. Reutelingsperger, L. Hofstra, J. Narula, J. Nucl. Med. **46**, 2051–2056 (2005)

L. Hegyi, S.J. Hardwick, R.C. Siow, J.N. Skepper, J. Hematother. Stem Cell Res. **10**, 27–42 (2001)

T. Ito, S. Yamada, M. Shiomi, Exp. Anim. **53**, 339–346 (2004)

R.K. Jain, J. Control. Release **53**, 49–67 (1998)

F.D. Kolodgie, H.K. Gold, A.P. Burke, D.R. Fowler, H.S. Kruth, D.K. Weber, A. Farb, L.J. Guerrero, M. Hayase, R. Kutys, J. Narula, A.V. Finn, R. Virmani, N. Engl. J. Med. **349**, 2316–2325 (2003a)

F.D. Kolodgie, A. Petrov, R. Virmani, N. Narula, J.W. Verjans, D.K. Weber, D. Hartung, N. Steinmetz, J.L. Vanderheyden, M.A. Vannan, H.K. Gold, C.P. Reutelingsperger, L. Hofstra, J. Narula, Circulation **108**, 3134–3139 (2003b)

F.D. Kolodgie, R. Virmani, A.P. Burke, A. Farb, D.K. Weber, R. Kutys, A.V. Finn, H.K. Gold, Heart **90**, 1385–1391 (2004)

S.C. Lee, M. Ruegsegger, P.D. Barnes, B.R. Smith, M. Ferrari, in *The Nanotechnology Handbook*, ed by B. Bhushan (Springer, Heidelberg, Germany, 2004a), pp. 279–322

S.C. Lee, M. Ruegsegger, M. Ferrari, in *The Encyclopedia of Nanoscience and Nanotechnology*, ed. by H.S. Nalwa (American Scientific Publishers, Stevenson Ranch, CA, 2004b)

W. Li, A. Hellsten, L.S. Jacobsson, H.M. Blomqvist, A.G. Olsson, X. M. Yuan, J. Mol. Cell. Cardiol. **37**, 969–978 (2004)

P. Libby, G. Sukhova, R.T. Lee, Z.S. Galis, J. Cardiovasc. Pharmacol. **25**(Suppl 2), S9–12 (1995)

C. Liu, G. Bhattacharjee, W. Boisvert, R. Dilley, T. Edgington, Am. J. Pathol. **163**, 1859–1871 (2003)

F. Lupu, N. Moldovan, J. Ryan, D. Stern, N. Simionescu, Blood Coagul. Fibrinolysis **4**, 743–752 (1993)

H. Maeda, T. Sawa, T. Konno, J. Cont. Release **74**, 47–61 (2001)

M. McAuliffe, F. Lalonde, D. McGarry, W. Gandler, K. Csaky, B. Trus, in *IEEE Computer-based Medical Systems (CBMS)* (2001), pp. 381–386

M. Meuwissen, A.C. van der Wal, K.T. Koch, C.M. van der Loos, S. A. Chamuleau, P. Teeling, R.J. de Winter, J.G. Tijssen, A.E. Becker, J.J. Piek, Am. J. Med. **114**, 521–527 (2003)

N.I. Moldovan, L. Moldovan, N. Simionescu, Blood Coagul. Fibrinolysis **5**, 921–928 (1994)

P.R. Moreno, K.R. Purushothaman, M. Sirol, A.P. Levy, V. Fuster, Circulation **113**, 2245–2252 (2006)

M. Naghavi, P. Libby, E. Falk, S.W. Casscells, S. Litovsky, J. Rumberger, J.J. Badimon, C. Stefanadis, P. Moreno, G. Pasterkamp, Z. Fayad, P.H. Stone, S. Waxman, P. Raggi, M. Madjid, A. Zarrabi, A. Burke, C. Yuan, P.J. Fitzgerald, D.S. Siscovick, C.L. de Korte, M. Aikawa, K.E. Juhani Airaksinen, G. Assmann, C.R. Becker, J.H. Chesebro, A. Farb, Z.S. Galis, C. Jackson, I.K. Jang, W. Koenig, R.A. Lodder, K. March, J. Demirovic, M. Navab, S.G. Priori, M.D. Rekhter, R. Bahr, S.M. Grundy, R. Mehran, A. Colombo, E. Boerwinkle, C. Ballantyne, W. Insull Jr., R.S. Schwartz, R. Vogel, P.W. Serruys, G.K. Hansson, D.P. Faxon, S. Kaul, H. Drexler, P. Greenland, J.E. Muller, R. Virmani, P.M. Ridker, D.P. Zipes, P.K. Shah, J.T. Willerson, Circulation **108**, 1664–1672 (2003)

N. Nighoghossian, L. Derex, P. Douek, Stroke **36**, 2764–2772 (2005)

J. Riemer, H.H. Hoepken, H. Czerwinska, S.R. Robinson, R. Dringen, Anal. Biochem. **331**, 370–375 (2004)

S.G. Ruehm, C. Corot, P. Vogt, S. Kolb, J.F. Debatin, Circulation **103**, 415–422 (2001)

E.A. Schellenberger, A. Bogdanov Jr., D. Hogemann, J. Tait, R. Weissleder, L. Josephson, Mol. Imaging **1**, 102–107 (2002)

M. Shiomi, T. Ito, S. Yamada, S. Kawashima, J. Fan, Arterioscler. Thromb. Vasc. Biol. **23**, 1239–1244 (2003)

P.K. Smith, R.I. Krohn, G.T. Hermanson, A.K. Mallia, F.H. Gartner, M.D. Provenzano, E.K. Fujimoto, N.M. Goeke, B.J. Olson, D.C. Klenk, Anal. Biochem. **150**, 76–85 (1985)

V.E. Stoneman, M.R. Bennett, Clin. Sci. (Lond) **107**, 343–354 (2004)

H.W. Strauss, M. Dunphy, N. Tokita, J. Nucl. Med. **45**, 1106–1107 (2004)

R. Weissleder, G. Elizondo, J. Wittenberg, C. Rabito, H. Bengele, L. Josephson, Radiology **175**, 489–493 (1990a)

R. Weissleder, P. Reimer, A.S. Lee, J. Wittenberg, T.J. Brady, AJR Am J Roentgenol **155**, 1161–1167 (1990b)